Design of 600-W Low-Loss Ultra-Wideband Ferriteless Balun

Chi Van Pham, *Student Member, IEEE*, Anh-Vu Pham, *Senior Member, IEEE*, and Robert E. Leoni, III, *Member, IEEE*

***Abstract*— We present the development of a low-loss, high-power, and ferriteless balun that operates over 0.1–1.6 GHz bandwidth. The proposed balun employs a novel compensated circuit, a single quarter-wave semirigid coaxial cable and an on-board inductor on a thermoset ceramic board to achieve high power and ultrawide bandwidth performance. The experimental results show that the balun achieves a measured average insertion loss of less than 0.5 dB and return loss of better than 10 dB from 100 MHz to more than 1.6 GHz. Within the measured bandwidth, the amplitude and phase imbalances are within ±1 dB and ±5°, respectively. Multiphysics analysis and high-power measurements demonstrate that the balun can handle more than 600 W and above at 1.6 GHz. To the best of our knowledge, the reported balun has the highest measured power handling capability per the largest 16:1 bandwidth ratio to date.**

***Index Terms*— Defected ground structure (DGS), multiphysics analysis, power handling capability, semirigid coaxial cable, transmission line (TL) balun, wide bandwidth balun.**

I. Introduction

HIGH power, wide bandwidth, low-loss, and compact baluns with an average power handling capability (APHC) of more than 500 W are used in push–pull amplifiers for wireless base stations, broadcast transmitters, air traffic control systems, and multifunctional radar systems [1]–[4]. Marchand compensated transmission line (TL) concepts [5]–[12] are widely used to design wide bandwidth baluns on printed circuit boards (PCBs). Other techniques including parallel- and serial-connected coaxial lines [13]–[18], ferrite coupled-coil lines [19], [20], and coaxial lines loaded with bulky ferrite cores [21] have been used to extend the balun bandwidth. Phelan [13] and Roberts [14] connected a single coaxial section with another short parallel solid rod and serial coaxial TL to obtain a good input matching over two widely separated frequencies. Dunn *et al.* [16] machined coaxial cables to have a larger characteristic impedance of the coaxial line to achieve a 13:1 bandwidth ratio (BWR). Note that these baluns have at least two $\lambda/4$ coaxial sections to maintain symmetry at balanced ports. Their sizes become excessively large at low frequencies. To operate at low frequencies down to a few megahertz's, a typical coaxial balun loads its $\lambda/4$ coaxial line with ferrite beads that enhance the inductance per unit length, consequently increasing the characteristic impedance of the coaxial TL [21]–[23]. Coupled-wire baluns are formed by winding a coaxial cable in N turns to enhance inductance by a factor N^2, resulting in a very large balun structure [19], [20]. Recently, to realize a compact size and broadband performance, multilayered planar baluns employing defected ground structures (DGSs) have been proposed but only operated at low power levels [6], [9]. While the multilayered baluns in [6]–[10] achieve broadband and low-loss performance, they are not suitable for high power applications because those balun topologies use broadside coupled TLs. The broadside coupled-line on multilayered thin films has small trace width and a narrow gap (25–50 μm) between the top and bottom conductors for tight coupling. The small gap required to achieve electrical performance suffers high electric field breakdown in high power applications [24].

High power and wide bandwidth baluns employing ferrite cores have been reported for CW-signals smaller than 200-W power between 0.1 and 2 GHz [19]–[23]. In these baluns, a ferrite core with high permeability is used with a conventional quarter-wavelength TL to convert a single-ended signal into a balanced one. The power handling capabilities of the ferrite baluns [21]–[23] are limited by the ferrite materials that suffer high losses and magnetic saturation [25]. The ferrite, dielectric, and conductive losses produce internal heat that contributes to the circuit breakdown of the coaxial baluns [24], [26], [27]. The power handling capability also depends on the glass transition temperature of the substrate material and coaxial dielectric [28], [29]. Ferriteless baluns [3], [4] with power handling capabilities from 500 to 700 W have been reported, but have a narrow operating bandwidth. The nonferrite high-power balun in [4] uses conventional quarter-wavelength coaxial cables on ceramic substrates to achieve a BWR of 2:1 around a center frequency of 725 MHz. To date, wide bandwidth (above 5:1 BWR) and high-power handling baluns (more than 500 W) have not been reported. Also, the power handling capability of the coaxial baluns has not been thoroughly investigated.

In this paper, we present a modified coaxial balun that can achieve simultaneously ultra-wideband (16:1 BWR), low loss, compact, and high-power handling of more than 600 W. For the first time, the DGS and the compensated inductor techniques are applied to a high-power coaxial-type balun to achieve both wide bandwidth and high-power handling

Manuscript received June 1, 2017; revised August 29, 2017; accepted September 30, 2017. Date of publication November 27, 2017; date of current version February 5, 2018. This work was supported by the Raytheon Company. *(Corresponding author: Chi Van Pham.)*

C. V. Pham and A.-V. Pham are with the Electrical and Computer Engineering Department, University of California at Davis, Davis, CA 95616 USA (e-mail: cvpham@ucdavis.edu; pham@ece.ucdavis.edu).

R. E. Leoni, III is with Integrated Defense Systems, Raytheon Company, Andover, MA 01810 USA.

Color versions of one or more of the figures in this paper are available online at http://ieeexplore.ieee.org.

Digital Object Identifier 10.1109/TMTT.2017.2764085

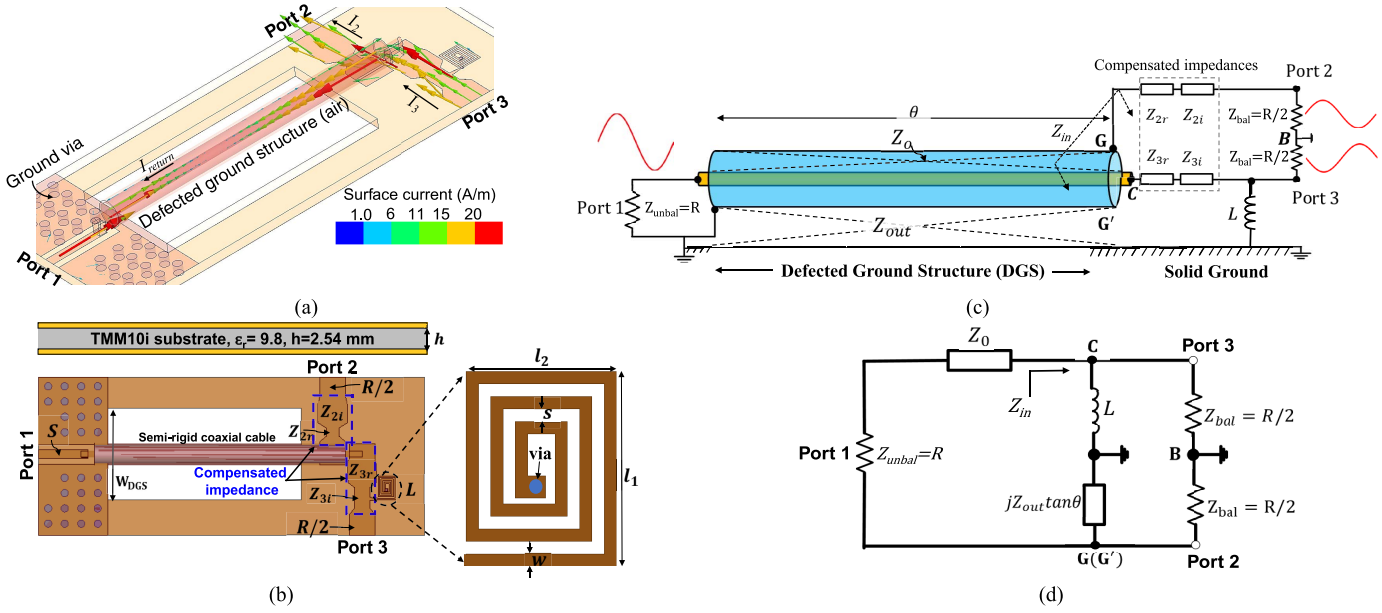

Fig. 1. Proposed wide bandwidth and high-power balun. (a) 3-D view with the surface current flow. (b) Cross section and top view. (c) Circuit diagram. (d) TL equivalent circuit without compensated impedances Z_{2r}, Z_{2i}, Z_{3r}, and Z_{3i}.

capabilities. The balun is implemented using only one quarter-wavelength semirigid coaxial cable on a rectangular defected substrate. An on-board inductor and compensated sections are designed to enhance the balun balances and to transform the impedance of balanced ports. The new balun topology avoids the use of broadside coupled-lines having small gaps and solely relies on the ultralow loss semirigid coaxial cable and a high thermal ceramic substrate to form the state-of-the-art 600-W balun. We also report the theoretical and comprehensive multiphysics analysis and characterization of APHCs, thermal stress, structural integrity, and electrical performance of the proposed balun. Finally, we have conducted high power measurements with a thermal infrared camera to validate that the balun can handle up to 600 W at 1.6 GHz without any electrical and structural breakdown.

This paper is structured as follows. Section II of this paper presents the design analysis of the proposed balun. In this section, the balun model and its equivalent circuit are analyzed to develop design procedures and demonstrate electrical performance. This section also provides a study of power handling capabilities of the balun using both theoretical derivation and multiphysics simulations. Section III shows electrical and high power measurements to validate the balun prototype. Finally, the conclusion is presented in Section IV.

II. Design of the 600-W Ferriteless Balun

A. Balun Operation and Impedance Bandwidth Analysis

Fig. 1 shows the proposed high power and wide bandwidth coaxial TL balun, its schematic and an equivalent circuit model. This balun consists of a semirigid coaxial cable sitting on a single layer ceramic board with a rectangular-shaped defected ground substrate. The modified DGS width is W_{DGS}, while the coaxial cable has an outer diameter of 6.4 mm and a length of 75 mm provided by Micro-Coax. The characteristic impedance and electrical length of the coaxial TL are denoted as Z_0 and θ, respectively. The balun balanced ports (Ports 2 and 3) have a compensated on-board spiral inductor L at Port 3 and compensated impedances, Z_{2r}, Z_{2i} and Z_{3r}, Z_{3i} for Ports 2 and 3, respectively. As the on-board inductor plays a major role in the impedance bandwidth at very low frequencies, the ideal inductor value is used to derive the bandwidth equation of the balun. When analyzing the imbalances of the balun, however, the self-resonance behavior can affect the phase and amplitude differences over the bandwidth. Therefore, a microstrip inductor model incorporating its self-resonance frequency is used in circuit simulation and analysis.

Fig. 1(a) and (c) shows a 3-D cross section view and circuit diagram of the balun. A traveling wave from Port 1 sees a symmetric path that consists of Port 2, Port 3, and a parasitic TL between the coaxial metallic shield and the PCB ground plane. Inside the semirigid coaxial TL, the signal, and ground return waves are always out-of-phase, and they each travel down to balanced ports in an odd-mode propagation. At the balanced ports, I_2 and I_3 have the same magnitude but are out of phase to form balanced signals. The symbols $Z_{\mathrm{unbal}} = R$ and $Z_{\mathrm{bal}} = R/2$ represent the terminating impedance of the unbalanced port and balanced ports, respectively, while Z_{out} is the characteristic impedance of the parasitic TL between the outer conductor of the semirigid coaxial cable to the PCB ground. Z_{out} must be much larger than R to minimize current return (I_{return}), resulting in a wide bandwidth impedance match at the unbalanced port. The compensating inductor and impedances (Z_{2r}, Z_{2i}, Z_{3r}, and Z_{3i}) improve the balance of the balun, resulting in maximum bandwidth performance.

Using the TL equations from [30], the circuit diagram in Fig. 1(c) is simplified as an equivalent circuit in Fig. 1(d)

that neglects compensated impedances Z_{2r}, Z_{2i}, Z_{3r}, and Z_{3i}. Considering G' and G are the same for the sake of drawing the circuit diagram. The impedance looking into G', which is the TL Z_{out} with the other end shorted at Port 1, is $jZ_{\text{out}}\tan\theta$. Assuming the TL is lossless [11], [30], Z_{in} in Fig. 1(d) can be derived to evaluate the bandwidth of the proposed balun as

$$Z_{\text{in}} = R_{\text{in}} + jX_{\text{in}} = \frac{(jZ_{\text{out}}\tan\theta)\frac{R}{2}}{jZ_{\text{out}}\tan\theta + \frac{R}{2}} + \frac{(j\omega L)\frac{R}{2}}{j\omega L + \frac{R}{2}} = Z_1 + Z_2 \tag{1}$$

$$Z_{\text{in}} = R_{\text{in}} + jX_{\text{in}} = \left(\frac{2RZ_{\text{out}}^2\tan^2\theta}{R^2 + 4Z_{\text{out}}^2\tan^2\theta} + \frac{2R\omega^2L^2}{R^2 + 4\omega^2L^2}\right) + j\left(\frac{R^2Z_{\text{out}}\tan\theta}{R^2 + 4Z_{\text{out}}^2\tan^2\theta} + \frac{R^2\omega L}{R^2 + 4\omega^2L^2}\right) \tag{2}$$

where $\theta = \pi f/(2f_0)$ and f_0 is a center frequency of the operating bandwidth of the balun. The proposed balun uses a single coaxial section with a length of a quarter-wavelength calculated at $f_0 = 1$ GHz.

Normalizing, Z_{in} relative to $R/2$, $z_n = r_n + jx_n = 2Z_{\text{in}}/R$ and let $\alpha = 2Z_{\text{out}}\tan\theta/R$ and $\beta = 2\omega L/R$, then r_n and x_n are given by

$$r_n = \frac{2R_{\text{in}}}{R} = \frac{\alpha^2}{1+\alpha^2} + \frac{\beta^2}{1+\beta^2} \tag{3}$$

$$x_n = \frac{2X_{\text{in}}}{R} = \frac{\alpha}{1+\alpha^2} + \frac{\beta}{1+\beta^2}. \tag{4}$$

The voltage reflection coefficient (Γ) and voltage standing wave ratio (VSWR) are calculated as

$$\Gamma = \frac{z_n - 2}{z_n + 2} = \frac{x_n^2 + r_n^2 - 4}{x_n^2 + (r_n+2)^2} + j\frac{4x_n}{x_n^2 + (r_n+2)^2} \tag{5}$$

$$\text{VSWR} = \frac{1+|\Gamma|}{1-|\Gamma|}. \tag{6}$$

The perfect input matching for the balun will be achieved if $Z_{\text{in}} = Z_0 = Z_{\text{unbal}} = R$. To satisfy these conditions in theory, $\alpha \to \infty$ and $\beta \to \infty$, meaning that Z_{out} and L need to be as large as possible over the operating bandwidth while Z_{unbal} is designed to match with Z_o.

Using (1) to (6), Fig. 2(a) and (b) shows calculated VSWR of the proposed balun with varying inductor values when $Z_{\text{out}} = 130\ \Omega$ and with varying Z_{out} when $L = 33$ nH. It can be observed that the bandwidth of the balun (for VSWR < 2) gets wider when L and Z_{out} are higher. If L increases from 10 to 40 nH [Fig. 2(a)], the matching bandwidth extends from 0.3 GHz down to 0.15 GHz or the balun doubles its BWR. The matching bandwidth at high frequency is quite constant to Z_{out} and L. In the case of varying Z_{out}, the VSWR gets smaller at high and low frequencies for larger values of Z_{out} [Fig. 2(b)].

To achieve a high Z_{out}, a DGS is developed in the balun. The DGS is formed by removing both the dielectric material and metal ground underneath the substrate in the vicinity of the coaxial line. Fig. 3 shows the extracted characteristic impedance of the parasitic TL for the DGS width using ANSYS HFSS: High Frequency Electromagnetic (EM) Field Simulation. Using the extracted characteristic impedance Z_{out}

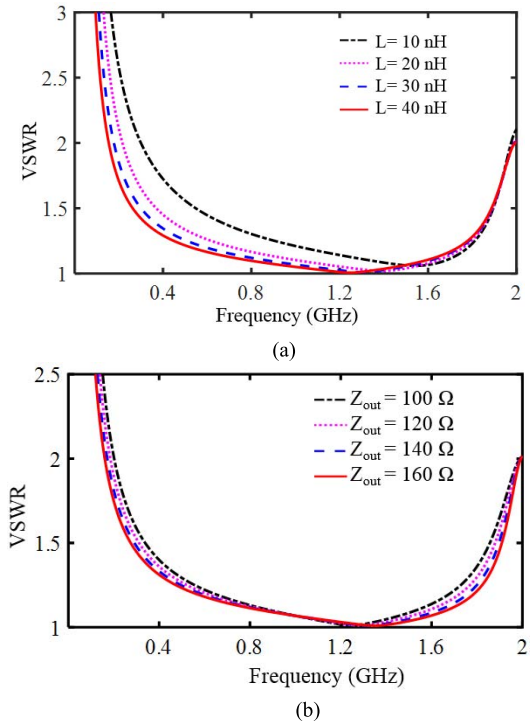

Fig. 2. Calculated VSWR of the proposed balun. (a) $Z_{\text{out}} = 130\ \Omega$ and varying L. (b) $L = 33$ nH and varying Z_{out}.

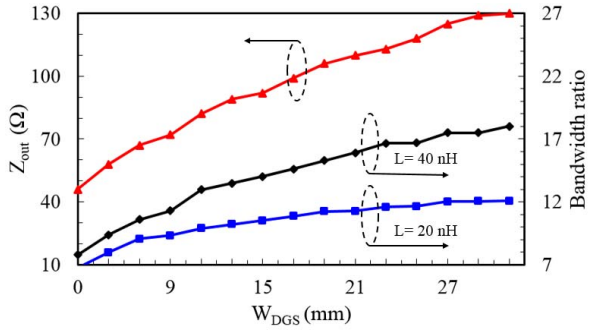

Fig. 3. Extracted characteristic impedance Z_{out} and the BWR of the proposed balun.

the simulation of the circuit model in Fig. 1(d) is conducted in Advanced Design System (ADS) software to calculate the BWR of the proposed balun for $L = 20$ nH and $L = 40$ nH. The BWR is defined as, BWR $= f_H/f_L$, where f_H is the high cutoff frequency of the balun's passband when the insertion loss (IL) is equal to 1 dB, and f_L is the low 1-dB cutoff frequency. As seen in Fig. 3, Z_{out} and BWR proportionally increase with respect to the defected area width and then saturate when $W_{\text{DGS}} > 27$ mm. Also, higher inductor values give larger BWRs. In summary, L and Z_{out} effectively control the matching bandwidth at low and high frequencies, respectively. To extend the high cutoff frequency f_H, the larger Z_{out} is desired by increasing the width of the DGS. A higher value of inductance L could extend the low cutoff frequency f_L down to megahertz ranges. The center frequency of the balun is scalable by adjusting the length of the semirigid coaxial cable. Noted that L and Z_{out} should be designed as large as possible to achieve wide bandwidth and to keep output

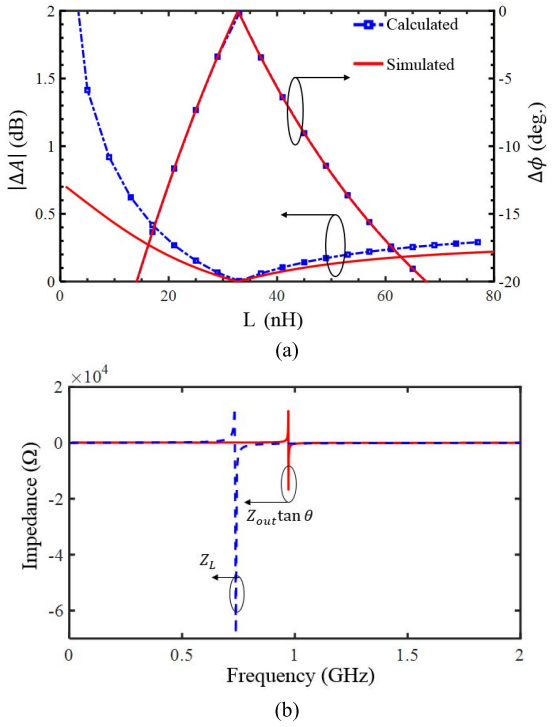

Fig. 4. (a) Calculated and simulated amplitude and phase imbalances at $f = 0.1$ GHz when varying inductor and $Z_{\text{out}} = 130\ \Omega$. (b) Extracted impedance from ANSYS HFSS simulations.

signals balanced at the same time. Analysis of imbalances of the balun will be detailed in Section II-B.

B. Analysis of Imbalances

Assuming the balun circuit in Fig. 1(d) is symmetrical between Ports 2 and 3 with respect to Port 1, the TL Z_0 can be removed to ease of the imbalance analysis. The balun ports are all terminated with R ($Z_{\text{bal}} = Z_{\text{unbal}} = R$). From S-parameter definitions [11], [30]: $S_{21} = 2V_2/V_1$ and $S_{31} = 2V_3/V_1$, where V_1 is the source voltage at unbalanced port and V_2 and V_3 are the voltage at Port 2 and Port 3, respectively. V_2 and V_3 are determined with respect to V_1 using voltage division

$$V_2 = \frac{V_1 Z_2}{Z_1 + Z_2 + R} \tag{7}$$

$$V_3 = \frac{V_1 Z_1}{Z_1 + Z_2 + R} \tag{8}$$

where $Z_1 = (j\omega L)//R$ and $Z_2 = (jZ_{\text{out}} \tan\theta)//R$. Using (7) and (8), the phase imbalance ($\Delta\phi = 180° - |\angle(S_{31}) - \angle(S_{21})|$) and amplitude imbalance ($\Delta A = \text{dB}(|S_{31}|) - \text{dB}(|S_{21}|)$) of the balun in Fig. 1(d) can be calculated as

$$\Delta\phi = 180° - \left| \angle\left(\frac{2Z_1}{Z_1 + Z_2 + R}\right) - \angle\left(\frac{2Z_2}{Z_1 + Z_2 + R}\right) \right| \tag{9}$$

$$\Delta A = \text{dB}\left|\frac{2Z_1}{Z_1 + Z_2 + R}\right| - \text{dB}\left|\frac{2Z_2}{Z_1 + Z_2 + R}\right|. \tag{10}$$

It can be expected from (9) and (10) that the amount of amplitude and phase imbalances converge to zero when L and Z_{out} both become very large (for which $Z_1 = Z_2 = R/2$). As a result, high values of L and Z_{out} properly reduce the imbalances of the balun at low frequencies. Fig. 4(a) shows

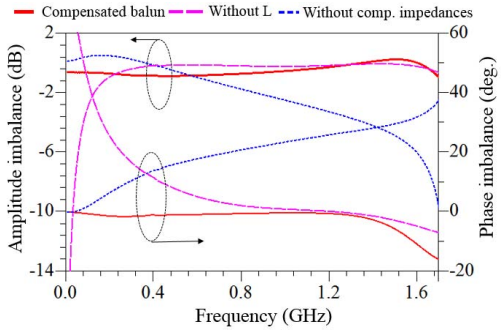

Fig. 5. Simulated imbalances of the balun without the inductor alone, without compensated impedances alone, and with inductor and compensated impedance all together using ANSYS HFSS.

the calculated and simulated imbalances of the balun circuit in Fig. 1(d) with varying inductor values, while $Z_{\text{out}} = 130\ \Omega$ at $f = 0.1$ GHz and with $f_0 = 1$ GHz. The calculated results of the imbalances agree with those of circuit simulations in ADS. The inductance is determined by two criteria: input impedance matching and phase and amplitude imbalances. An infinitely large inductance could improve input impedance matching at frequency ranges below 1 GHz [Fig. 2(a)], but will drastically degrade the imbalances of the balun shown in Fig. 4(a). Here, the minimum theoretical values of phase and amplitude imbalances are achieved with $L = 33$ nH, resulting in $Z_L = Z_{\text{out}} \tan(\pi f/2f_0) = 21\ \Omega$ with $f_0 = 1$ GHz.

The realized 35-nH spiral inductor has a simulated self-resonance frequency of 738 MHz. To achieve good balances in theory, the two output branches should satisfy the condition: $Z_L = 2\pi f_0 L_{\text{eff}} = Z_{\text{out}} \tan(\pi f/2f_0) = Z_{\text{out}} \tan\theta$, where L_{eff} is an effective inductance. However, $Z_{\text{out}} \tan\theta$ does not align with Z_L over the entire operating band. Fig. 4(b) plots the full-wave EM simulation of impedances $Z_{\text{out}} \tan\theta$ and Z_L. Here, the HFSS simulation of the semirigid coaxial TL with an actual length over the defected ground is conducted. Then, input impedance $Z_{\text{stub}} = Z_{\text{out}} \tan\theta$ of the semi-rigid coaxial line is extracted. As seen in Fig. 4(b), the "transition frequency" of $Z_{\text{out}} \tan\theta$ is at 971 MHz. After the self-resonance frequency of the spiral inductor at 738 MHz, the impedance differences between Z_L and $Z_{\text{out}} \tan\theta$ become large. Therefore, the additional impedances at Ports 2 and 3 are used to compensate for the phase and amplitude imbalances. These compensated impedances also reduce the effect of the discontinuity reactance created by the coaxial line to microstrip transitions. The discontinuities become significant above 1 GHz. For these reasons, the compensated impedances in a tapered structure are employed [12], [18].

The impedances (Z_{2r}, Z_{2i}, Z_{3r}, and Z_{3i}) are used to compensate for the phase and amplitude imbalances when the balun is interfaced with coaxial connectors. In our design, we start with low characteristic impedance around 25 Ω because the balun is designed for 25 Ω at the balanced ports. We then tune the impedance values to get a good phase and amplitude imbalances ($|\Delta\phi| < 10°$) and ($|\Delta A| < 1$ dB) at high frequency (1.6 GHz). Fig. 5 shows simulated imbalances of the proposed balun with both the spiral inductor and

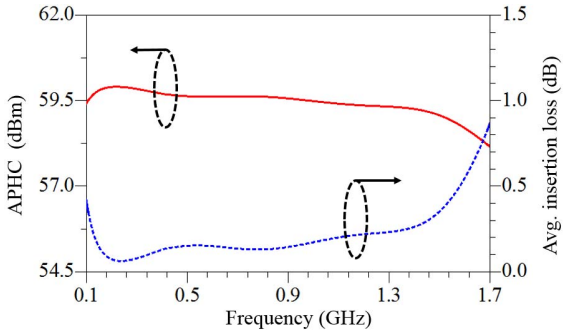

Fig. 6. Calculated APHC of the proposed balun using (11).

compensated impedances at balanced ports, without the inductor, and without the compensated impedances. To have $|\Delta\phi| < 10°$ and $|\Delta A| < 1$ dB, the balun limits its operating bandwidth from 0.4 to 1.6 GHz without the inductor and from 1 MHz to 0.3 GHz without using compensated impedances. In the case of a fully compensated balun, the bandwidth extends from 1 MHz to 1.6 GHz. In summary, the on-board inductor and output compensated impedances significantly improve the balances of the proposed balun over its operating bandwidth.

C. Multiphysics Analysis of Power Handling Capabilities

1) Theoretical Power Handling Capability: To analyze thermal performance of the balun under a very high power CW signal (500–1000 W), we first estimate APHC with respect to transmission losses and the glass transition temperature (T_g). The thermal profile on the balun depends on the heat distortion temperature of copper, the ceramic substrate material, and the dielectric of the coaxial cable. Using a heat transfer analysis method [28], [29], the APHC of the proposed balun can be numerically calculated as follows:

$$P_{\text{APHC}} = \frac{T_g - T_{\text{amb}}}{\Delta T + \frac{\Gamma_{\text{avg}}}{2Ah_c}} \tag{11}$$

where T_{amb} is the room temperature, $2A$ is the whole top and bottom surface area of the TMM10i substrate neglecting defected substrate area (air), $h_c = 10$ W/m^2°C is the natural convection heat transfer coefficient, and ΔT is the generated temperature [24]. Γ_{avg} is the average transmission loss calculated from the full-wave HFSS simulation. As expected from (11), the balun can handle the highest power when its substrate material and coaxial cable have the lowest loss and the highest glass transition temperature. Therefore, we have chosen an ultralow loss semirigid coaxial cable (UT-250C-ULL) and a thermoset substrate, TMM10i that has high glass transition temperature of 590 °C, high thermal conductivity of 0.76 W/m/K and high breakdown electric strength of 2×10^6 V/m. Fig. 6 shows the calculated APHC using (11) and the HFSS-simulated average IL of the balun (IL $= -10\log_{10}(|S_{12}|^2 + |S_{13}|^2)$ (dB)). The calculated APHC of the proposed TMM10i balun is ~59.6 dBm (912 W) at 0.6 GHz and ~58.7 dBm (741 W) at 1.6 GHz and is reduced at higher frequencies as the transmission loss of the balun increases.

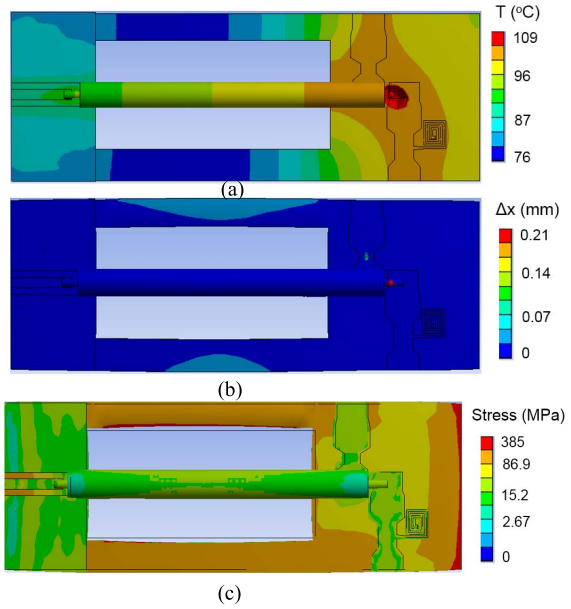

Fig. 7. Coaxial balun with 590-W input power at 0.6 GHz. (a) Temperature rise profile. (b) 3-D deformation distribution. (c) 3-D thermal stress.

The peak power handling capability (PPHC) of the proposed balun is determined by the dielectric strength of the substrate, the dielectric of the connector and semirigid cable [26]. The electric strength of the TMM10i substrate and Teflon PTFE is on the order of 20 and 10 kV/mm, respectively. Thus, the PPHC of the proposed balun very much depends on the electric strength of Teflon PTFE, which is the dielectric of the semirigid coaxial cable. The ultralow loss coaxial cable (UT-250C-ULL) has an estimated PPHC of 1482.9 W at 1 GHz.

In addition, there are two regions of the proposed balun sensitive to a corona discharge.

1) The gap formed between the microstrip trace and top ground at the unbalanced input port where the electric strength of input signal has its maximum intensity. We have increased the critical gap for high power operation while still maintaining the balun electrical performance.
2) The dielectric between the inner and outer conductors of the semirigid coaxial cable. The dielectric of the cable has a low-loss tangent and a much higher dielectric strength than air (3 kV/mm). The properties of the dielectric will protect the coaxial cable against corona discharge [2].

2) Comprehensive Multiphysics Analysis of Power Handling Capability: We have conducted comprehensive multiphysics ANSYS analysis to determine power handling, temperature rise, local hot spot, and the thermal stress of the balun as a function of input power. The temperature rise and deformed mesh are fed back into an EMs model to analyze the corresponding electrical changes of the proposed coaxial balun. Fig. 7 shows the temperature rise and structural deformation profiles of the proposed balun with the input power of 590 W at 0.6 GHz. In the coupled EMs—thermal-structural analysis, the dielectric loss of the semirigid coaxial cable

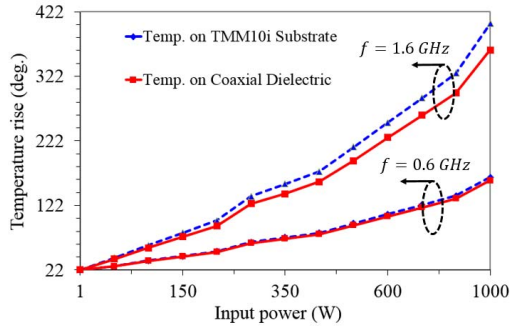

Fig. 8. Temperature rise profile on the substrate and coaxial dielectric material of the proposed balun using multiphysics ANSYS simulations.

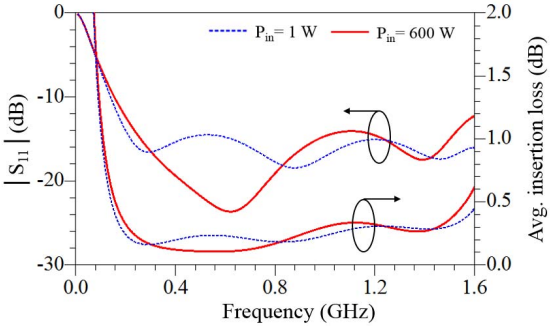

Fig. 9. Return loss and IL of the proposed balun with the input power of 1 and 600 W.

increases with temperature. Thus, the thermal and stress profiles will vary with the feedback temperature rise, resulting in a converged maximum temperature of 104 °C along the cable dielectric material and 108 °C at the junction of the coaxial cable and microstrip trace near the output. Also, a maximum deformation of 0.1 mm occurs along the balun edge-sides and will not affect the balun performance over its low-frequency bandwidth below 2 GHz. Fig. 7(c) shows the equivalent (von-Mises) stress profiles of the proposed balun. The thermal stress mostly happens at the inner conductor to the microstrip interface and output balance ports. Along the TMM10i substrate, the Von-mises stress is 175 MPa, which is below the material yield strength limit (280 MPa).

Fig. 8 shows the maximum temperature rise in the TMM10i substrate and the dielectric material of the semirigid coaxial cable. Because the coaxial dielectric material (low-density PTFE) has a glass transition temperature of T_o = 262 °C, the balun can handle up to 670 W at 1.6 GHz and more than 1000 W at 0.6 GHz. The EM model of the balun updates the feedback deformed mesh at different power levels and provides simulated power-dependent S-parameters to verify electrical performance. Fig. 9 shows a full-wave EM simulation with the input power of 1 W and 600 W for comparison. It can be seen that there is an expected frequency shift of 19 MHz with P_{in} = 600 W. The reference frequency is the lowest frequency (f = 0.1 GHz) at 1 W input power.

III. Electrical and High Power Measurements

A. Realization of the High Power and Ultra-Wideband Balun

We have designed and fabricated the proposed high power and wide bandwidth balun to achieve a BWR of higher than 15 at a center frequency f_0 = 1 GHz. The unbalanced port and balanced port impedances are chosen as Z_{unbal} = 50 Ω and Z_{bal} = 25 Ω, respectively. The calculated circuit parameters are given as L = 35 nH, W_{DGS} = 30 mm, and Z_{out} = 130 Ω. The designed spiral inductor [Fig. 1(b)] includes three turns with l_1 = 7 mm, l_2 = 5.5 mm, w = 0.45 mm, and s = 0.45 mm. The balun is fabricated on a Rogers TMM10i substrate with a dielectric constant (ε_r) of 9.8 and a thickness (h) of 2.54 mm. Table I summarizes the final dimension values of each impedance. Fig. 10 shows the connectorized balun prototype with the size of 116 mm × 47 mm × 2.54 mm.

TABLE I
Impedance Design Summary

Parameter	R	$R/2$	Z_{2i}	Z_{2r}	Z_{3i}	Z_{3r}
Impedance (Ω)	50	25	19	28	26	19
Microstrip width (mm)	2.54	7.9	8.8	3.9	4.7	8.8
Microstrip length (mm)	15	6	5	2.6	2.8	5

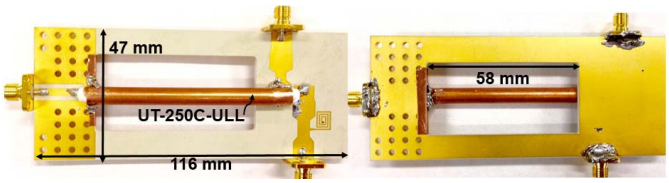

Fig. 10. Prototype of the ferriteless balun. (a) Top view. (b) Bottom view.

B. Electrical Measurements

Three test ports (Ports 1, 2, and 3) of the four-port network analyzer (PNA-X N5247A) were used to evaluate the small-signal electrical performance of the balun. Guided short-open-load-thru multiport calibration available from the Keysight PNA-X N5247A was performed for three ports using coaxial standards. In the three-port calibration, each test port was connected to the short standard, open standard, and load standard. Then, a thru standard connection was made between port pairs (Ports 1 and 2, Ports 1 and 3).

Fig. 11 shows the measured, full-wave simulated, and circuit simulated return losses, average ILs, and phase and amplitude imbalances of the balun. The circuit simulation uses an ADS microstrip model of the rectangular spiral inductor that includes the self-resonance behavior. It can be observed that the circuit model and full-wave simulations can predict the trend of the balun performance well. The return loss of the balun is better than 10 dB from 0.1 GHz to beyond 1.6 GHz. The balun achieves a measured average IL of less than 1 dB from 0.1 to 1.6 GHz. Fig. 11(b) shows that a measured phase difference of ±5° is achieved from 10 MHz to greater than 1.6 GHz and an amplitude imbalance of less than ±0.5 and ±1 dB is well maintained from 650 MHz to 1.6 GHz and from 30 MHz to 1.6 GHz, respectively. Fig. 11(c) shows a good agreement between the simulation and measurement of the $|S_{22}|$, $|S_{33}|$, $|S_{21}|$, $|S_{31}|$, phase (S_{21}), and phase (S_{31}).

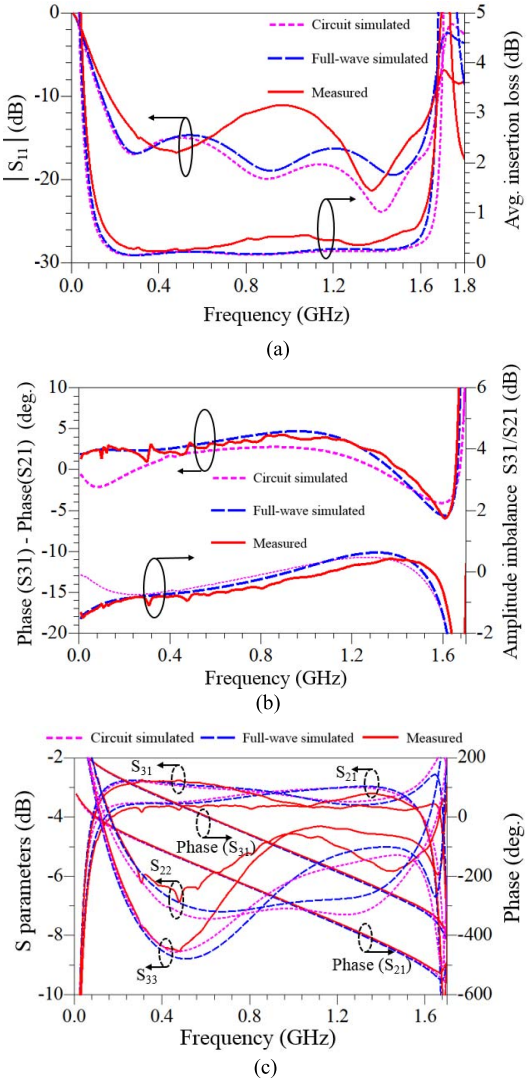

Fig. 11. Measured results of the balun. (a) Return losses and average ILs. (b) Phase and amplitude imbalances. (c) $|S_{22}|$, $|S_{33}|$, $|S_{21}|$, $|S_{31}|$, phase (S_{21}), and phase (S_{31}).

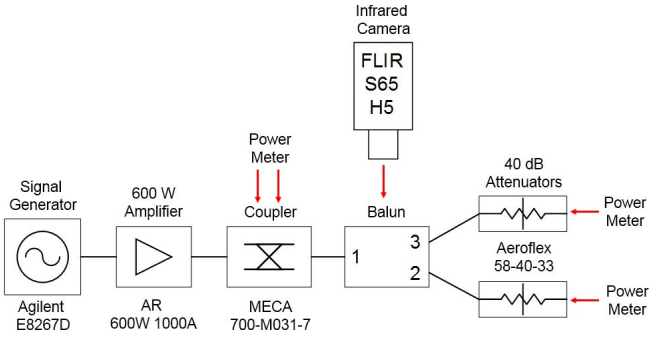

Fig. 12. High-power test setup.

C. High-Power Handling Measurement

We have conducted the measurements of the balun prototype with high power input signals. Fig. 12 shows the block diagram set-up of the high power measurements. The test set-up includes a 600%W tube amplifier, high power

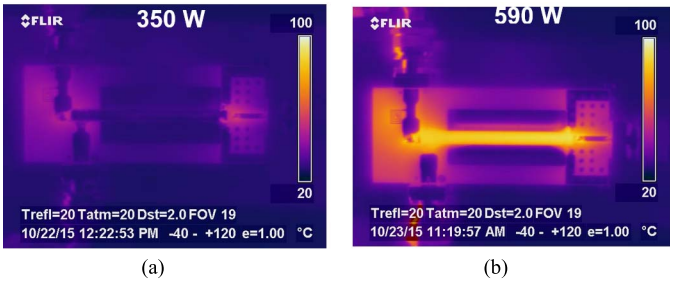

Fig. 13. Measured infrared image at 600 MHz with input power. (a) 350 W. (b) 590 W.

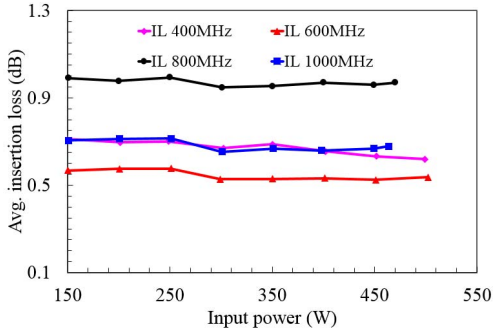

Fig. 14. Measured average IL under varied input power.

hybrid couplers, 40-dB attenuators, and a thermal infrared camera (FLIR S65-H5) to capture the relative temperature rise profile in the balun. A CW signal has been applied to the balun at ambient pressure ($p = 1000$ mbar) and temperature ($T_{\text{am}} = 22$ °C) and was swept over frequency and power ranges. For each frequency, the test system recorded the incident power (P_1) and transmitted power (P_2 and P_3) and took an infrared image of the balun at the same time. Then, the average IL (avg. IL) of the balun is calculated by

$$IL_{\text{avg. IL}} = -10\log_{10}\left(2\sqrt{\frac{P_2P_3}{P_1^2}}\right). \tag{12}$$

Fig. 13 shows the measured temperature distribution on the balun for 350 and 590 W input signals at 600 MHz. As compared with the simulated temperature rise profile [Fig. 7(a)], the maximum hot spot can be clearly identified close to the input and output coaxial junctions as well as at the on-board inductor with $P_{\text{in}} = 600$ W at 600 MHz, measured $T_{\max} = 100$ °C compared with simulated $T_{\max} = 109$ °C. The difference can be due to the ambient temperature around the balun and no heat sink being considered for the high power measurement. In short, the simulated temperature correlates with that obtained from measurements.

Fig. 14 shows the measured average ILs of the balun with a varying input power at different frequencies. The measured average IL is calculated from the measured data from power sensors using (12). It can be observed that the measured average ILs remain constant over the input power range. Compared with Fig. 11(a), the IL is ~0.1 dB higher because of using three N-type connectors and adapters for high power measurement.

TABLE II
COMPARISON OF HIGH-POWER BALUN DESIGN

Design	Frequency (GHz)	Amplitude (dB) / Phase Imbalance (°)	Size in λ_g @ f_0	Topology/Power handling (P)
[3]	1-2	1/10	0.2 x 0.25	Ferriteless, P< 500 W
[4]	0.45-0.76	1/10	0.2 x 0.25	Ferriteless, P< 700 W
[6]	0.05-2.3	1/8	0.19 x 0.28	Coupled-line, P < 10 W
[9]	0.08-1.86	0.4/10	0.22 x 0.22	Coupled-line, P <15 W
[10]	1-9	1/8	0.1 x 0.06	Coupled-line, P< 15 W
[17]	0.1-1	1/10	0.16 x 0.27	Ferriteless, P< 40 W
[19]	0.1-2.8	0.3/0.6	0.1 x 0.06	Coupled-coil, P < 80 W
[22]	0.01-0.5	1/10	0.1 x 0.05	Ferrite, P < 100 W
This work	0.1-1.6	1 /5	0.12 x 0.29	Ferriteless, P> 600 W

Table II compares the proposed balun with the other reported broadband high power baluns with an average IL of 1 dB. Compared to published ferriteless baluns, our proposed balun has the combined highest power handling and BWR.

IV. CONCLUSION

In this paper, the design and development of an ultra-wideband balun for high power microwave applications have been demonstrated. The multiphysics simulations are employed to design the balun in terms of high power, electrical responses, and structural integrity. A ferriteless coaxial balun model is designed and prototyped using only one quarter-wavelength coaxial section and DGSs to achieve a BWR of 16:1. Our experimental results show that the proposed balun can handle up to 600-W input power. To the best of our knowledge, the proposed balun achieves the highest combined power handling and BWR.

REFERENCES

[1] G. N. Saddik, R. S. Singh, and E. R. Brown, "Ultra-wideband multifunctional communications/radar system," *IEEE Trans. Microw. Theory Techn.*, vol. 55, no. 7, pp. 1431–1437, Jul. 2007.

[2] K. Shamsaifar, T. Rodriguez, and J. Haas, "High-power combline diplexer for space," *IEEE Trans. Microw. Theory Techn.*, vol. 61, no. 5, pp. 1850–1860, May 2013.

[3] A. Maekawa, T. Yamamoto, E. Mitani, and S. Sano, "A 500 W push-pull AlGaN/GaN HEMT amplifier for L-band high power application," in *IEEE MTT-S Int. Microw. Symp. Dig.*, Jun. 2006, pp. 722–725.

[4] J. He, J. H. Qureshi, W. Sneijers, D. A. Calvillo-Cortes, and L. C. N. deVreede, "A wideband 700 W push-pull Doherty amplifier," in *IEEE MTT-S Int. Microw. Symp. Dig.*, May 2015, pp. 1–4.

[5] N. Marchand, "Transmission line conversion transformers," *Electronics*, vol. 17, no. 12, pp. 142–145, Dec. 1944.

[6] C. Van Pham, B. Pham, A.-V. Pham, and R. E. Leoni, "A 46⋆1 bandwidth ratio balun on multilayer organic substrate," in *IEEE MTT-S Int. Microw. Symp. Dig.*, May 2015, pp. 1–3.

[7] A. C. Chen, A.-V. Pham, and R. E. Leoni, "A novel broadband even-mode matching network for Marchand baluns," *IEEE Trans. Microw. Theory Techn.*, vol. 57, no. 12, pp. 2973–2980, Dec. 2009.

[8] A. C. Chen, A.-V. Pham, and R. E. Leoni, III, "Development of low-loss broad-band planar baluns using multilayered organic thin films," *IEEE Trans. Microw. Theory Techn.*, vol. 53, no. 11, pp. 3648–3655, Nov. 2005.

[9] B. L. Pham, H. H. Ta, A.-V. Pham, R. E. Leoni, and Y. Leviatan, "23:1 bandwidth ratio quasi-lumped component balun on a multilayer organic substrate," *IET Microw., Antennas Propag.*, vol. 10, pp. 561–567, Apr. 2016.

[10] H. H. Ta, B. Le Pham, and A.-V. Pham, "Compact wide bandwidth balun based on modified asymmetric broadside coupled lines," *IEEE Microw. Wireless Compon. Lett.*, vol. 22, no. 12, pp. 624–626, Dec. 2012.

[11] R. Phromloungsri, M. Chongcheawchamnan, and I. D. Robertson, "Inductively compensated parallel coupled microstrip lines and their applications," *IEEE Trans. Microw. Theory Techn.*, vol. 54, no. 9, pp. 3571–3582, Sep. 2006.

[12] R. Chadha and K. C. Gupta, "Compensation of discontinuities in planar transmission lines," *IEEE Trans. Microw. Theory Techn.*, vol. MTT-30, no. 12, pp. 2151–2156, Dec. 1982.

[13] H. R. Phelan, "A wide-band parallel-connected balun," *IEEE Trans. Microw. Theory Techn.*, vol. MTT-18, no. 5, pp. 259–263, May 1970.

[14] W. K. Roberts, "A new wide-band balun," *Proc. IRE*, vol. 45, pp. 1628–1631, Dec. 1957.

[15] R. Bawer and J. J. Wolfe, "A printed circuit balun for use with spiral antennas," *IRE Trans. Microw. Theory Techn.*, vol. MTT-8, pp. 319–325, May 1960.

[16] D. A. Dunn, J. W. McLaughlin, and R. W. Grow, "A wide-band balun," *IRE Trans. Microw. Theory Techn.*, vol. MTT-6, no. 3, pp. 314–316, Jul. 1958.

[17] R. M. Smith, J. Lees, P. J. Tasker, J. Benedikt, and S. C. Cripps, "A 40 W push-pull power amplifier for high efficiency, decade bandwidth applications at microwave frequencies," in *IEEE MTT-S Int. Microw. Symp. Dig.*, Jun. 2012, pp. 1–3.

[18] G. Oltman, "The compensated balun," *IEEE Trans. Microw. Theory Techn.*, vol. MTT-14, no. 3, pp. 112–119, Mar. 1966.

[19] J. Horn and G. Boeck, "Ultra wideband balun for power applications," in *Proc. 34th Eur. Microw. Conf. (EuMC)*, Oct. 2004, pp. 369–371.

[20] G. A. Hofbauer, "An ultra-wideband microwave balun using a tapered coaxial coil structure working from kHz range to beyond 26.5 GHz," in *IEEE MTT-S Int. Microw. Symp. Dig.*, Jun. 2005, pp. 551–554.

[21] A. K. Ezzeddine and H. C. Huang, "10 W ultra-broadband power amplifier," in *IEEE MTT-S Int. Microw. Symp. Dig.*, Jun. 2008, pp. 643–646.

[22] J. Cho *et al.*, "Design of a 100 watt high-efficiency power amplifier for the 10–500 MHz band," in *Proc. IEEE Asia–Pacific Microw. Conf. (APMC)*, Dec. 2009, pp. 285–288.

[23] H. Noto, K. Yamauchi, M. Nakayama, M. Kohama, and Y. Hirano, "A broadband 200 W GaN push–pull power amplifier enhanced second harmonic suppression with point-symmetric 2-stage baluns," in *Proc. Eur. Microw. Integr. Circuits Conf. (EuMIC)*, Oct. 2011, pp. 252–255.

[24] I. J. Bahl and K. C. Gupta, "Average power-handling capability of microstrip lines," *IEE J. Microw., Opt. Acoust.*, vol. 3, no. 1, pp. 1–4, Jan. 1979.

[25] M/A-COM Inc. (2016). *Transformers/Baluns*. [Online]. Available: http://www.macom.com/products/passives/transformers–baluns

[26] M. A. Sánchez-Soriano, M. Edwards, Y. Quéré, D. Andersson, S. Cadiou, and C. Quendo, "Mutiphysics study of RF/microwave planar devices: Effect of the input signal power," in *Proc. 15th Int. Conf. Thermal, Mech. Multiphys. Simulation Experim. Microelectron. Microsyst. (EuroSimE)*, Apr. 2014, pp. 1–7.

[27] H. H. J. M. Janssen, E. J. W. ter Maten, and D. van Houwelingen, "Simulation of coupled electromagnetic and heat dissipation problems," *IEEE Trans. Magn.*, vol. 30, no. 5, pp. 3331–3334, Sep. 1994.

[28] Y. J. Cheng, K. Wu, and W. Hong, "Power handling capability of substrate integrated waveguide interconnects and related transmission line systems," *IEEE Trans. Adv. Packag.*, vol. 31, no. 4, pp. 900–909, Nov. 2008.

[29] M. Á. Sánchez-Soriano, Y. Queré, V. Le Saux, C. Quendo, and S. Cadiou, "Average power handling capability of microstrip passive circuits considering metal housing and environment conditions," *IEEE Trans. Compon., Packag., Manuf. Technol.*, vol. 4, no. 10, pp. 1624–1633, Oct. 2014.

[30] D. M. Pozar, *Microwave Engineering*, 2nd ed. Hoboken, NJ, USA: Wiley, 1998.

Chi Van Pham (S'12) received the B.E. degree (with highest Hons.) in electronics and telecommunications engineering from the Hanoi University of Science and Technology, Hanoi, Vietnam, in 2012, and the M.S. degree in electrical and computer engineering from the University of California at Davis, Davis, CA, USA, in 2015, where he is currently pursuing the Ph.D. degree.

His current research interests include applied electromagnetics, wideband passive devices and antenna design, specifically the development of high power components, and systems for radars and energy harvesting applications.

Mr. Pham is a Fellow of the Vietnam Education Foundation. He was a recipient of the IEEE MTT-S Fellowship Award in 2016.

Anh-Vu Pham (SM'03) received the B.E.E. degree (with highest Hons.), M.S., and Ph.D. degrees in electrical engineering from the Georgia Institute of Technology, Atlanta, GA, USA, in 1995, 1997, and 1999, respectively.

He joined the University of California at Davis, Davis, CA, USA, as an Assistant Professor in 2002, and became a Full Professor in 2008. From 1999 to 2002, he was an Assistant Professor with Clemson University, Clemson, SC, USA. He is conducting research in microwave and millimeter-wave integrated circuit design, power amplifiers, electronic packaging, sensors, energy harvesting, and phased-array antennas. His research was supported by the DARPA, NSF, ONR, AFRL, and numerous companies. He has authored ∼160 peer-reviewed papers, several book chapters, and 2 books.

Dr. Vu was the recipient of the National Science Foundation CAREER Award in 2001 and the 2008 Outstanding Young Engineer Award from the IEEE Microwave Theory and Techniques Society. He served as the Chair of the IEEE Microwave Theory and Techniques Technical Coordinate Committee on Microwave and Millimeter Packaging from 2003 to 2006, and the Chair of the IEEE MTT-S International Microwave Symposium Technical Committee on Power Amplifiers and Integrated Devices. He was a Microwave Distinguished Lecturer of the IEEE MTT-S from 2010 to 2012. He was the Co-Chair of the Technical Program Committee for the IEEE MTT-S International Microwave Symposium, San Francisco, CA, USA, in 2016, and is the Co-Chair of the Technical Program Committee for the IEEE Asia–Pacific Microwave Conference. He is currently a Co-Director of the Davis Millimeter Wave Research Center. He co-founded RF Solutions, a fabless semiconductor company providing power amplifiers and RFICs for WiFi applications. RF Solutions was acquired by Anadigics in 2003. In 2008, he co-founded and served as the CTO of Planarmag Inc., which was acquired by TE Connectivity in 2010.

Robert E. Leoni, III (M'98) received the Ph.D. degree in electrical engineering from Lehigh University, Bethlehem, PA, USA, in 1998.

He joined the Raytheon Company, Andover, MA, USA, where he is currently an Engineering Fellow with the Microelectronics Engineering and Technology Department. He possesses 20 years' experience in III–V technology and application research and development. He currently leads several efforts related to the optimization of GaN PAs and microwave transmitters.